IUCrData

ISSN 2414-3146

3,5,6-Trichloropyridin-2-ol

Tashonda M. Vaughn,[a] Saneei Soheil,[a] Olalekan M. Ogundele,[b] Frank R. Fronczek[c] and Rao M. Uppu[a]*

[a]Department of Environmental Toxicology, Southern University and A&M College, Baton Rouge, Louisiana 70813, USA, [b]Department of Comparative Biomedical Sciences, School of Veterinary Medicine, Louisiana State University, Baton Rouge, Louisiana 70810, USA, and [c]Department of Chemistry, Louisiana State University, Baton Rouge, LA 70803, USA. *Correspondence e-mail: rao_uppu@subr.edu

Received 13 November 2024
Accepted 19 November 2024

Edited by W. T. A. Harrison, University of Aberdeen, United Kingdom

Keywords: crystal structure; chlorpyrifos; triclopyr derivatives.

CCDC reference: 2403937

Structural data: full structural data are available from iucrdata.iucr.org

The title compound, $C_5H_2Cl_3NO$, is almost planar. In the crystal, the molecules form centrosymmetric hydrogen-bonded dimers through pairwise O—H···N interactions to generate $R_2^2(8)$ loops.

3D view

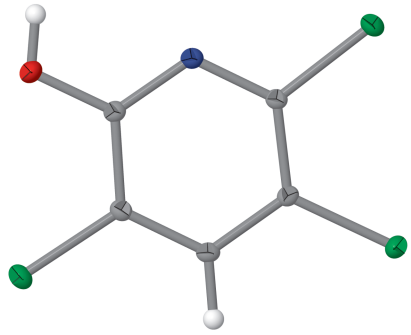

Chemical scheme

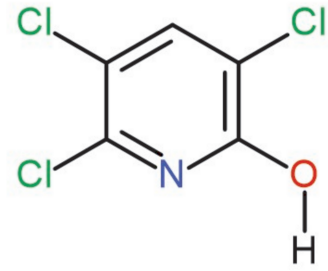

Structure description

3,5,6-Trichloro-2-pyridinol (TCP, $C_5H_2Cl_3NO$) is the primary degradation product of chlorpyrifos (CPP, $C_9H_{11}Cl_3NO_3PS$) and chlorpyrifos-methyl (CPFM, $C_7H_7Cl_3NO_3PS$), two of the most widely used organophosphate insecticides in agriculture (Bouchard *et al.*, 2011). TCP has been shown to intensify the toxic effects of CPF(*M*), leading to endocrine disruption, cellular toxicity, and organ damage (Gao *et al.*, 2021; Li *et al.*, 2020). It enhances the impact of CPF(*M*) on testosterone synthesis and Sertoli cell function by inhibiting testosterone binding to androgen receptors, furthering hormonal disruption through pathways involving luteinizing hormone and signaling molecules such as CREB and Star, essential for testosterone production. TCP also downregulates genes critical for spermatogenesis, posing potential risks to male fertility (Mansukhani *et al.*, 2024). Molecular modeling indicates that TCP interacts with sex-hormone-binding globulin, potentially aggravating hormonal imbalances (Hazarika *et al.*, 2019).

Beyond endocrine effects, TCP exhibits direct cytotoxicity (Gao *et al.*, 2021) and may bind to DNA in a groove-binding manner similar to Hoechst, possibly favoring specific base-pair regions without significantly distorting the DNA structure (Bailly *et al.*, 1993; Bucevičius *et al.*, 2018; Kashanian *et al.*, 2012). Studies have demonstrated substantial cellular damage in human embryonic kidney cells (HEK 293) following TCP exposure, signaling a risk of kidney toxicity (Van Emon *et al.*, 2018). TCP is further linked to hepatotoxicity and nephrotoxicity in animal models, where it accumulates in vital organs and may cause structural and functional damage (Deng *et al.*, 2016). Additionally, age-

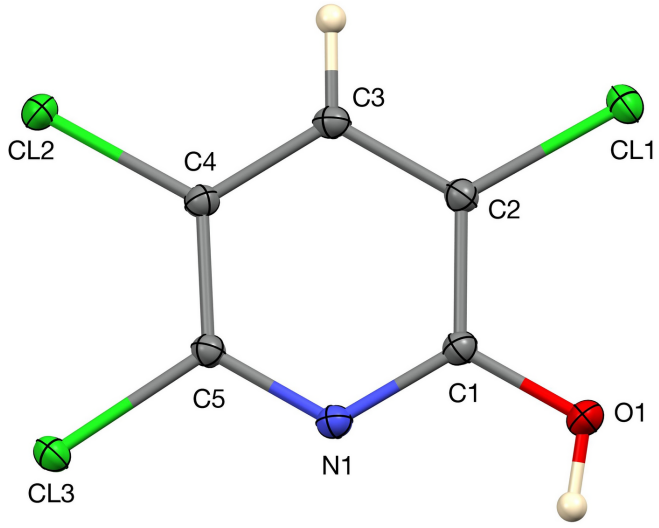

Figure 1
The asymmetric unit of TCP with 50% displacement ellipsoids.

dependent sensitivity to TCP has been observed, with pre-weanling rats displaying heightened vulnerability due to pharmacokinetic differences (Timchalk *et al.*, 2002).

TCP is notable for its long half-life in soil, ranging from 65 to 360 days depending on environmental conditions, and its high solubility in water (80.9 mg l^{-1}), facilitating contamination of surface and groundwater (Zhao *et al.*, 2017; Timchalk *et al.*, 2002). This persistence raises substantial concerns about bioaccumulation, biomagnification, and ecosystem disruption, especially in aquatic environments where TCP has been found to be toxic to organisms (Echeverri-Jaramillo *et al.*, 2020; Van Emon *et al.*, 2018). TCP levels in human urine serve as biomarkers for CPF(*M*) exposure, aiding in occupational and environmental exposure assessments (Bouchard *et al.*, 2011).

In the United States, the EPA revoked all food-related uses of CPF(*M*) in 2021, effectively banning its use on crops intended for human consumption; however, a November 2023 court ruling temporarily reinstated CPF(*M*) tolerances while the EPA reconsiders its decision (EPA, 2023). In the European Union, both CPF and CPFM were banned in 2020, with strict limits on residue levels in food (EFSA, 2020). As of 2024, CPF(*M*) remains restricted for non-food uses in some areas, with existing stocks allowed under controlled conditions, though further bans and stricter regulations are anticipated. While these restrictions are in place, it is important to note that TCP can also result from the soil and microbial degradation of triclopyr, triclopyr butoxyethyl ester and triclopyr triethylamine salt, three commonly used pyridine-based herbicides for managing woody plants, vines, and broadleaf weeds (Cessna *et al.*, 2002; Deng *et al.*, 2016; Dias *et al.*, 2017). The primary concern with these herbicides is non-target toxicity.

Table 1
Hydrogen-bond geometry (Å, °).

D—H···A	D—H	H···A	D···A	D—H···A
O1—H1···N1^{i}	0.821 (19)	1.919 (19)	2.7371 (10)	174.3 (19)

Symmetry code: (i) $-x+1, -y+1, -z$.

Given its widespread relevance to human and animal health, and to support the identification of potential molecular targets in biological systems, we have investigated the crystal structure of TCP: it crystallizes in the monoclinc space group $P2_1/c$ with one molecule in the asymmetric unit (Fig. 1). The molecule is close to planar, with the six atoms of the pyridine ring lying a mean of 0.007 Å from their best plane. The Cl atoms lie out of this plane by an average of 0.058 Å, and the O atom lies 0.0430 (14) Å out of plane. The C—N distances are 1.3343 (11) and 1.3347 (11) Å, the C—Cl distances fall in the range 1.7189 (8)–1.7202 (8) Å and the C—O distance is 1.3207 (11) Å. In the crystal, the molecules form centrosymmetric hydrogen-bonded dimers through pairwise O—H···N interactions (Table 1) to generate $R_2^2(8)$ loops. No other directional interactions could be identified. The hydrogen-bonded dimer is shown in Fig. 2, and the unit cell is illustrated in Fig. 3.

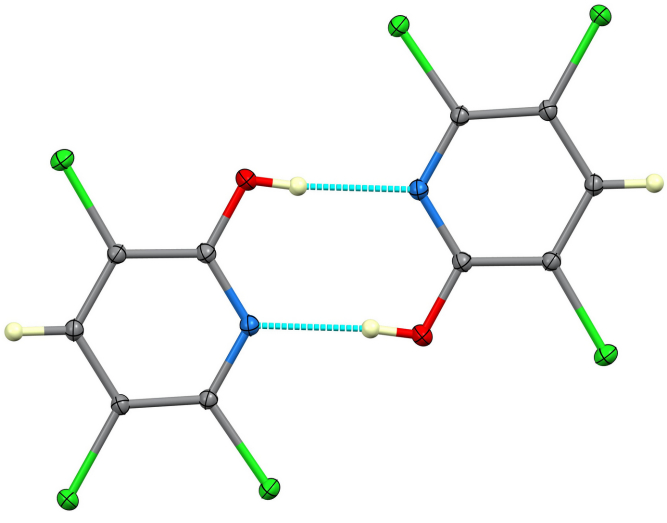

Figure 2
The centrosymmetric hydrogen-bonded dimer.

Synthesis and crystallization

3,5,6-Trichloro-2-pyridinol, $C_5H_2Cl_3NO$ (CAS 6515–38-4) was obtained from AmBeed (Arlington Heights, Illinios, USA) and was used without further purification. Crystals in the form of colorless laths were prepared by slow cooling of a nearly

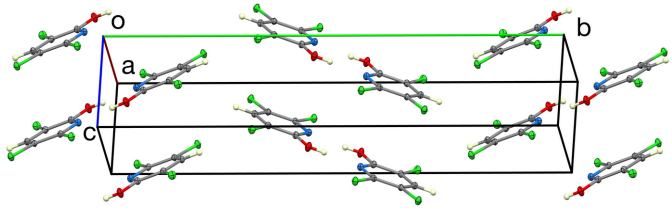

Figure 3
The unit-cell packing.

saturated solution of the title compound in boiling deionized water (resistance *ca*. 18 M cm^{-1}).

Refinement

Crystal data, data collection and structure refinement details are summarized in Table 2.

Table 2
Experimental details.

Crystal data	
Chemical formula	$C_5H_2Cl_3NO$
M_r	198.43
Crystal system, space group	Monoclinic, $P2_1/c$
Temperature (K)	100
a, b, c (Å)	6.1616 (3), 22.3074 (10), 5.0396 (2)
β (°)	99.356 (1)
V (Å^3)	683.47 (5)
Z	4
Radiation type	Ag $K\alpha$, λ = 0.56086 Å
μ (mm^{-1})	0.64
Crystal size (mm)	0.47 × 0.23 × 0.14
Data collection	
Diffractometer	Bruker D8 Venture DUO with Photon III C14
Absorption correction	Multi-scan (*SADABS*; Krause *et al.*, 2015)
T_{min}, T_{max}	0.840, 0.916
No. of measured, independent and observed [$I > 2\sigma(I)$] reflections	56728, 4816, 4626
R_{int}	0.035
(sin $\theta/\lambda)_{max}$ (Å^{-1})	0.944
Refinement	
$R[F^2 > 2\sigma(F^2)]$, $wR(F^2)$, S	0.034, 0.073, 1.33
No. of reflections	4816
No. of parameters	94
H-atom treatment	H atoms treated by a mixture of independent and constrained refinement
$\Delta\rho_{max}$, $\Delta\rho_{min}$ (e Å^{-3})	0.78, −0.50

Computer programs: *APEX4* and *SAINT* (Bruker, 2016), *SHELXT2018/2* (Sheldrick, 2015a), *SHELXL2019/1* (Sheldrick, 2015b), *Mercury* (Macrae *et al.*, 2020) and *publCIF* (Westrip, 2010).

Funding information

The authors acknowledge the support from the National Institutes of Health (NIH) through the National Institute of General Medical Sciences (NIGMS) Institutional Development Award (IDeA) grant No. P20 GM103424–21, the US Department of Education (US DoE; Title III, HBGI Part B grant No. P031B040030), and the National Science Foundation (NSF) under grant No. 1736136, CREST Center for Next Generation Multifunctional Composites (NextGen Composites Phase II). The purchase of the diffractometer was made possible by National Science Foundation MRI award CHE–2215262. The contents of the manuscript are solely the responsibility of authors and do not represent the official views of NIH, NIGMS, NSF, or US DoE.

References

Bailly, C., Colson, P., Hénichart, J. P. & Houssier, C. (1993). *Nucleic Acids Res.* **21**, 3705–3709.
Bouchard, M. F., Chevrier, J., Harley, K. G., Kogut, K., Vedar, M., Calderon, N., Trujillo, C., Johnson, C., Bradman, A., Barr, D. B. & Eskenazi, B. (2011). *Environ. Health Perspect.* **119**, 1189–1195.
Bruker (2016). *APEX4* and *SAINT*, Bruker AXS Inc., Madison, Wisconsin, USA.
Bucevičius, J., Gražvydas Lukinavičius, G. & Rūta Gerasimaitė, R. (2018). *Chemosensors* **6**, 18.
Cessna, A. J., Grover, R. & Waite, D. T. (2002). *Rev. Environ. Contam. Toxicol.* **174**, 19–48.
Deng, Y., Zhang, Y., Lu, Y., Zhao, Y. & Ren, H. (2016). *Sci. Total Environ.* **544**, 507–514.
Dias, J. L. C. S., Banu, A., Sperry, B. P., Enloe, S. F., Ferrell, J. A. & Sellers, B. A. (2017). *Weed Technol.* **31**, 928–934.
Echeverri-Jaramillo, G., Jaramillo-Colorado, B., Sabater-Marco, C. & Castillo-López, M. (2020). *Environ. Sci. Pollut. Res.* **27**, 32770–32778.
EFSA (2020). European Food Safety Authority. Chlorpyrifos and chlorpyrifos-methyl banned in the EU.
EPA (2023). Environmental Protection Agency. Court ruling on CPF tolerances.
Gao, H., Li, J., Zhao, G. & Li, Y. (2021). *Toxicology*, **460**, 152883.
Hazarika, J., Ganguly, M. & Mahanta, R. (2019). *J. Appl. Toxicol.* **39**, 1002–1011.
Kashanian, S., Shariati, Z., Roshanfekr, H. & Ghobadi, S. (2012). *DNA Cell Biol.* **31**, 1341–1348.
Krause, L., Herbst-Irmer, R., Sheldrick, G. M. & Stalke, D. (2015). *J. Appl. Cryst.* **48**, 3–10.
Li, J., Fang, B., Ren, F., Xing, H., Zhao, G., Yin, X., Pang, G. & Li, Y. (2020). *Sci. Total Environ.* **726**, 138496.
Macrae, C. F., Sovago, I., Cottrell, S. J., Galek, P. T. A., McCabe, P., Pidcock, E., Platings, M., Shields, G. P., Stevens, J. S., Towler, M. & Wood, P. A. (2020). *J. Appl. Cryst.* **53**, 226–235.
Mansukhani, M., Roy, P., Ganguli, N., Majumdar, S. S. & Sharma, S. S. (2024). *Pestic. Biochem. Physiol.* **204**, 106065.
Sheldrick, G. M. (2015). *Acta Cryst.* C**71**, 3–8.
Timchalk, C., Nolan, R. J., Mendrala, A. L., Dittenber, D. A., Brzak, K. A. & Mattsson, J. L. (2002). *Toxicol. Sci.* **66**, 34–53.
Van Emon, J. M., Pan, P. & van Breukelen, F. (2018). *Chemosphere*, **191**, 537–547.
Westrip, S. P. (2010). *J. Appl. Cryst.* **43**, 920–925.
Zhao, Y., Wendling, L. A., Wang, C., & Pei, Y. (2017). *J. Soils Sediments*, **17**, 889--900.

full crystallographic data

IUCrData (2024). **9**, x241126 [https://doi.org/10.1107/S2414314624011260X]

3,5,6-Trichloropyridin-2-ol

Tashonda M. Vaughn, Saneei Soheil, Olalekan M. Ogundele, Frank R. Fronczek and Rao M. Uppu

3,5,6-Trichloropyridin-2-ol

Crystal data

$C_5H_2Cl_3NO$
M_r = 198.43
Monoclinic, $P2_1/c$
a = 6.1616 (3) Å
b = 22.3074 (10) Å
c = 5.0396 (2) Å
β = 99.356 (1)°
V = 683.47 (5) Å^3
Z = 4
$F(000)$ = 392
D_x = 1.928 Mg m^{-3}
Ag $K\alpha$ radiation, λ = 0.56086 Å
Cell parameters from 9745 reflections
θ = 2.6–31.9°
μ = 0.64 mm^{-1}
T = 100 K
Lath fragment, colourless
0.47 × 0.23 × 0.14 mm

Data collection

Bruker D8 Venture DUO with Photon III C14 diffractometer
Radiation source: IμS 3.0 microfocus
φ and ω scans
Absorption correction: multi-scan (SADABS; Krause *et al.*, 2015)
T_{min} = 0.840, T_{max} = 0.916
56728 measured reflections
4816 independent reflections
4626 reflections with $I > 2\sigma(I)$
R_{int} = 0.035
θ_{max} = 32.0°, θ_{min} = 2.6°
h = −11→11
k = −42→42
l = −9→9

Refinement

Refinement on F^2
Least-squares matrix: full
$R[F^2 > 2\sigma(F^2)]$ = 0.034
$wR(F^2)$ = 0.073
S = 1.33
4816 reflections
94 parameters
0 restraints
Primary atom site location: dual
Hydrogen site location: mixed
H atoms treated by a mixture of independent and constrained refinement
$w = 1/[\sigma^2(F_o^2) + (0.0157P)^2 + 0.4001P]$ where $P = (F_o^2 + 2F_c^2)/3$
$(\Delta/\sigma)_{max}$ = 0.001
$\Delta\rho_{max}$ = 0.78 e Å^{-3}
$\Delta\rho_{min}$ = −0.50 e Å^{-3}

Special details

Geometry. All esds (except the esd in the dihedral angle between two l.s. planes) are estimated using the full covariance matrix. The cell esds are taken into account individually in the estimation of esds in distances, angles and torsion angles; correlations between esds in cell parameters are only used when they are defined by crystal symmetry. An approximate (isotropic) treatment of cell esds is used for estimating esds involving l.s. planes.

Refinement. Both H atoms were located in difference maps and the one on C was treated as riding in a geometrically idealized position with C—H distance = 0.95 Å, while the coordinates for the one on O were refined. Hydrogen displacement parameters were assigned as U_{iso}(H) = 1.2U_{eq} for the attached C atom and 1.5U_{eq} for the attached O atom.

Fractional atomic coordinates and isotropic or equivalent isotropic displacement parameters (Å²)

	x	*y*	*z*	U_{iso}*/U_{eq}
Cl1	0.93128 (4)	0.66668 (2)	0.00185 (5)	0.01441 (4)
Cl2	0.32839 (4)	0.69555 (2)	0.65348 (4)	0.01403 (4)
Cl3	0.17530 (4)	0.56134 (2)	0.51565 (5)	0.01375 (4)
O1	0.72509 (13)	0.54889 (3)	−0.08395 (16)	0.01555 (12)
H1	0.661 (3)	0.5167 (9)	−0.111 (4)	0.023*
N1	0.47368 (12)	0.55968 (3)	0.20415 (15)	0.01124 (10)
C1	0.63850 (14)	0.58150 (4)	0.09104 (17)	0.01105 (11)
C2	0.72170 (14)	0.63936 (4)	0.15463 (17)	0.01084 (11)
C3	0.62942 (14)	0.67423 (4)	0.33201 (17)	0.01121 (12)
H3	0.684573	0.713275	0.378054	0.013*
C4	0.45373 (14)	0.65136 (4)	0.44307 (17)	0.01050 (11)
C5	0.38383 (13)	0.59348 (4)	0.37596 (17)	0.01031 (11)

Atomic displacement parameters (Å²)

	U^{11}	U^{22}	U^{33}	U^{12}	U^{13}	U^{23}
Cl1	0.01297 (8)	0.01471 (8)	0.01651 (9)	−0.00232 (6)	0.00528 (6)	0.00075 (6)
Cl2	0.01719 (9)	0.01155 (7)	0.01464 (8)	−0.00103 (6)	0.00649 (6)	−0.00281 (6)
Cl3	0.01369 (8)	0.01177 (7)	0.01685 (8)	−0.00229 (6)	0.00571 (6)	0.00032 (6)
O1	0.0175 (3)	0.0118 (2)	0.0191 (3)	−0.0019 (2)	0.0083 (2)	−0.0045 (2)
N1	0.0115 (2)	0.0093 (2)	0.0132 (3)	−0.00046 (19)	0.0027 (2)	−0.0007 (2)
C1	0.0112 (3)	0.0095 (3)	0.0126 (3)	0.0002 (2)	0.0025 (2)	−0.0006 (2)
C2	0.0105 (3)	0.0103 (3)	0.0119 (3)	−0.0008 (2)	0.0023 (2)	0.0005 (2)
C3	0.0124 (3)	0.0090 (3)	0.0121 (3)	−0.0011 (2)	0.0017 (2)	−0.0003 (2)
C4	0.0116 (3)	0.0090 (3)	0.0110 (3)	0.0002 (2)	0.0022 (2)	−0.0006 (2)
C5	0.0103 (3)	0.0090 (3)	0.0117 (3)	−0.0005 (2)	0.0021 (2)	0.0002 (2)

Geometric parameters (Å, º)

Cl1—C2	1.7191 (8)	N1—C1	1.3347 (11)
Cl2—C4	1.7202 (8)	C1—C2	1.4063 (12)
Cl3—C5	1.7189 (8)	C2—C3	1.3757 (12)
O1—C1	1.3207 (11)	C3—C4	1.3937 (12)
O1—H1	0.821 (19)	C3—H3	0.9500
N1—C5	1.3343 (11)	C4—C5	1.3854 (11)
C1—O1—H1	110.9 (13)	C2—C3—H3	120.5
C5—N1—C1	119.73 (7)	C4—C3—H3	120.5
O1—C1—N1	120.16 (8)	C5—C4—C3	118.30 (7)
O1—C1—C2	119.06 (8)	C5—C4—Cl2	122.12 (6)
N1—C1—C2	120.78 (8)	C3—C4—Cl2	119.58 (6)
C3—C2—C1	119.55 (8)	N1—C5—C4	122.66 (8)
C3—C2—Cl1	120.69 (6)	N1—C5—Cl3	116.53 (6)
C1—C2—Cl1	119.73 (6)	C4—C5—Cl3	120.80 (6)
C2—C3—C4	118.95 (7)		

C5—N1—C1—O1	−178.44 (8)	C2—C3—C4—C5	1.98 (12)
C5—N1—C1—C2	1.22 (13)	C2—C3—C4—Cl2	−177.11 (7)
O1—C1—C2—C3	178.53 (8)	C1—N1—C5—C4	0.35 (13)
N1—C1—C2—C3	−1.14 (13)	C1—N1—C5—Cl3	−179.07 (7)
O1—C1—C2—Cl1	0.66 (12)	C3—C4—C5—N1	−1.97 (13)
N1—C1—C2—Cl1	−179.01 (7)	Cl2—C4—C5—N1	177.10 (7)
C1—C2—C3—C4	−0.50 (13)	C3—C4—C5—Cl3	177.43 (6)
Cl1—C2—C3—C4	177.35 (7)	Cl2—C4—C5—Cl3	−3.51 (11)

Hydrogen-bond geometry (Å, º)

D—H···*A*	*D*—H	H···*A*	*D*···*A*	*D*—H···*A*
O1—H1···N1^{i}	0.821 (19)	1.919 (19)	2.7371 (10)	174.3 (19)

Symmetry code: (i) −*x*+1, −*y*+1, −*z*.